JOURNAL OF CATALYSIS **167,** 470–481 (1997)
ARTICLE NO. CA971585

The Metathesis of Propylene Catalyzed by Model Oxides Studied Using a High-Pressure Reactor Incorporated into an Ultrahigh Vacuum Chamber

B. F. Bartlett, H. Molero, and W. T. Tysoe[1]

Department of Chemistry and Laboratory for Surface Studies, University of Wisconsin–Milwaukee, Milwaukee, Wisconsin 53211

Received June 13, 1996; revised December 16, 1996; accepted December 18, 1996

The olefin metathesis activity of a series of model catalysts consisting of metallic molybdenum, MoO_2, or MoO_3 is investigated using a combined high-pressure reactor/ultrahigh vacuum apparatus. The model catalysts are analyzed using X-ray and ultraviolet photoelectron, Raman, and Auger spectroscopies and it is shown that MoO_2 is the most active above ~650 K. Reaction in this temperature regime proceeds with a high activation energy (~60 kcal/mol). Another, lower-activation-energy (~6 kcal/mol) regime is encountered for reaction below ~650 K and it is suggested that both reactions proceed simultaneously. In addition, the absolute rate and selectivity for the reaction on MoO_2 below 650 K are similar to those found for high loadings of supported molybdenum oxide, suggesting that an oxide layer provides a good model catalyst for this reaction. It is also found that reaction proceeds in the presence of a thick carbonaceous layer where the thickness of this layer decreases with increasing oxidation state. A Raman analysis of the surface of the catalyst following reaction indicates that this layer consists predominantly of hydrocarbon species, although a small amount of graphitic carbon is detected.

INTRODUCTION

An active heterogeneous catalyst for the metathesis of propylene,

$$2\ C_3H_6 \rightarrow C_2H_4 + C_4H_8,$$

was discovered in 1964 by Banks and Bailey (1) and consists of alumina-support molybdenum oxide. It was soon found that the reaction could also be catalyzed in homogeneous phase (2) and it has been suggested, in this case, that the reaction proceeds via the initial formation of a carbene which acts as the "active site" for catalysis. This is proposed to react further with an alkene forming a metallacycle which can thermally decompose via the reverse of its formation pathway to yield metathesis products (3–22). While metallic molybdenum is not usually thought of as an active catalyst, it has been demonstrated that metallic molybdenum can catalyze this reaction at sufficiently high temperatures (>650 K) (23). In this case, the reaction activation energy is ~65 kcal/mol, substantially higher than values found for supported molybdenum oxides. This paper addresses the effect of oxidation on the activity of molybdenum for olefin (specifically propylene) metathesis using a high-pressure reactor incorporated into an ultrahigh vacuum chamber. This strategy has the advantage that samples can be prepared and characterized and their catalytic activity measured without intervening exposure to air. Furthermore, this approach allows the nature of the catalyst surface to be monitored merely by removing the sample from the high-pressure reactor into ultrahigh vacuum. This strategy reveals that the surface of the catalyst is covered by carbonaceous deposits, and restart reactions (see below) show that the reaction proceeds in the presence of such a layer. *Ex situ* Raman analysis of the catalyst surface reveals that this layer consists primarily of strongly bound hydrocarbons as well as a small amount of graphitic carbon.

EXPERIMENTAL

The apparatus that was used for these experiments has been described in detail elsewhere (24, 25). Briefly, however, it consists of a bakeable, stainless-steel, ultrahigh vacuum chamber operating at a base pressure of 1×10^{-10} Torr following bakeout. It is equipped with a quadrupole mass analyzer for residual gas analysis, leak testing, and temperature-programmed desorption studies. It also contains a four-grid retarding-field analyzer (RFA) which can be used for low-energy electron diffraction (LEED) experiments or for collecting Auger spectra. It is also equipped with a rotatable hemispherical analyzer which was also used for Auger measurements by collecting the *n(E)* spectrum from electrons excited using a 3-kV incident electron beam, and the conventional *dn(E)/dE* spectrum is obtained by differentiating these data using a Savitzky–Golay algorithm.

The apparatus also includes a coaxial high-pressure reactor which can be sealed and filled to 1 atmosphere while

[1] To whom correspondence should be addressed. Fax: (414) 229-5530. E-mail: wtt@alpha2.csd.uwm.edu.

0021-9517/97 $25.00

maintaining ultrahigh vacuum ($\sim 2 \times 10^{-10}$) in the rest of the apparatus. This is attached to a recirculating loop and the gas recirculated by a pump. The pressure is monitored by means of a capacitance manometer and the gas composition analyzed by diverting aliquots of the gas mixture to a gas chromatograph. The reaction rate is measured directly from the product accumulation curve for low (<1%) conversions.

The molybdenum foil sample is attached to the end of the sample manipulator and can be resistively heated to ~2000 K or cooled to 80 K by thermal contact to a liquid-nitrogen-filled reservoir. The sample is cleaned using a standard procedure which consists of heating at 1450 K in 2.0×10^{-7} Torr of oxygen and the annealing at 2000 K *in vacuo* to remove any remaining oxygen. The sample is judged clean when no impurities (predominantly carbon) are detected using Auger spectroscopy.

Raman spectra were collected using a spectrometer comprising a Spex double monochromator where photons are detected using a Peltier-effect cooled photomultiplier operating in pulse-counting mode. Spectra were excited using either the 514.5- or 488.0-nm lines of an Argon ion laser and light was back scattered from the sample. The collection time for each scan was approximately 20 min, and several scans were averaged together to get each spectrum. The similarity of each scan was examined before averaging to eliminate the possibility of laser-induced alteration of the sample. The laser light was steered to the sample via two turning prisms and passed through an iris to remove plasma lines. However, due to the low signal intensity from the sample, these were still evident in some of the spectra and the laser light was then changed to prevent interference between Raman and plasma lines.

X-ray photoelectron spectra were collected using a VG EscaLab spectrometer and were excited using Mg $K\alpha$ radiation, and the photoemitted electrons were analyzed using a 100-mm radius hemispherical analyzer operating at a pass energy of 25 eV, yielding an overall spectral resolution of 0.8 eV.

Ultraviolet photoelectron spectra were obtained at the Wisconsin Synchrotron Radiation Center using the Aladdin storage ring. The stainless-steel, ultrahigh vacuum chamber used for these experiments operated at a base pressure of $\sim 1 \times 10^{-10}$ Torr following bakeout and was attached to the end of a Mark V Grasshopper monochromator. The chamber was equipped with a quadrupole mass analyzer for residual gas analysis and to test gas purities. It also contained a double-pass cylindrical mirror analyzer which was used to collect both Auger and photoelectron spectra. Auger spectra were excited using a 3-keV electron beam and the spectra collected by pulse counting the scattered electrons and the *dn(E)/dE* Auger spectrum obtained by numerically differentiating the *n(E)* signal. The analyzer was operated at a pass energy of 25 eV to collect photoelectron spectra and this yielded an overall spectral resolution of 0.15 eV. Photoelectron spectra were excited using 55-eV radiation.

The propylene used for these experiments (Linde, CP Grade) was transferred from the cylinder to a glass bottle and further purified by repeated bulb-to-bulb distillations, and its cleanliness monitored either mass spectroscopically or using the gas chromatograph. In all experiments, the high-pressure reactor was ballasted to 1 atmosphere using nitrogen to ensure that the gas circulation rate was identical for all experiments.

RESULTS

Sample Preparation and Characterization

The model catalysts used to probe variations in catalytic activity for olefin metathesis as a function of molybdenum oxidation state consisted of metallic molybdenum, MoO_2, and MoO_3. Metallic molybdenum can be obtained rather straightforwardly in ultrahigh vacuum using a conventional cleaning procedure as described above, which consists of heating in oxygen to remove any surface carbon and then annealing *in vacuo* to remove any remaining oxygen (26–28). The sample cleanliness is monitored, in this case, from the Auger spectrum of the sample which is judged clean when no oxygen or carbon signals are detected. The synthesis of MoO_2 by the controlled oxidation of metallic molybdenum has been well documented in the literature and these procedures were followed in this work (29–41). Oxidation was carried out in the ultrahigh vacuum portion of the chamber at a pressure 3×10^{-5} Torr of oxygen with the sample heated to 1130 K for a period of at least 70 s, although longer reaction times generally lead to thicker films. Figure 1 displays the Mo 3*d* photoelectron spectrum of a molybdenum foil that had been treated in this way as a function of oxidation time in 3×10^{-5} Torr of O_2 at a sample temperature of 1130 K. Metallic molybdenum exhibits a spin-orbit coupling split doublet with a $3d_{5/2}$ peak at 228.2 eV binding energy (BE) with a corresponding $2p_{3/2}$ peak at 231.3 eV. As oxidation proceeds, this peak attenuates in intensity so that after heating for 185 s the spectrum now exhibits peaks at 229.4 and 232.5 eV BE. The presence of the peak at 229.4-eV binding energy confirms the formation of molybdenum dioxide (42–46), although there is a very small feature present at 231.0 eV suggesting the formation of a very small amount of MoO_3. The results of annealing this film *in vacuo* are also documented in the data of Fig. 2. These data were collected by heating the sample for a period of 120 s to the temperature indicated adjacent to each spectrum and allowing the sample to cool to room temperature, following which the spectrum was recorded. These results indicate that MoO_2 is thermally stable *in vacuo* up to an annealing temperature of ~1200 K but is reduced to metallic molybdenum by heating to 1420 K. Note that while

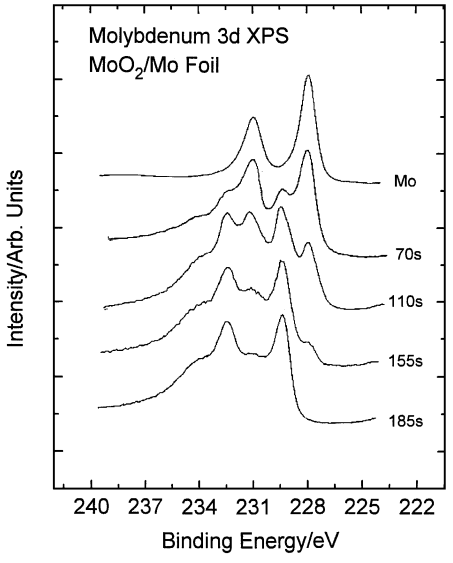

FIG. 1. X-ray photoelectron spectra of a molybdenum foil oxidized in 3×10^{-5} Torr of oxygen at 1130 K for various times. The reaction time is marked adjacent to each of the spectra.

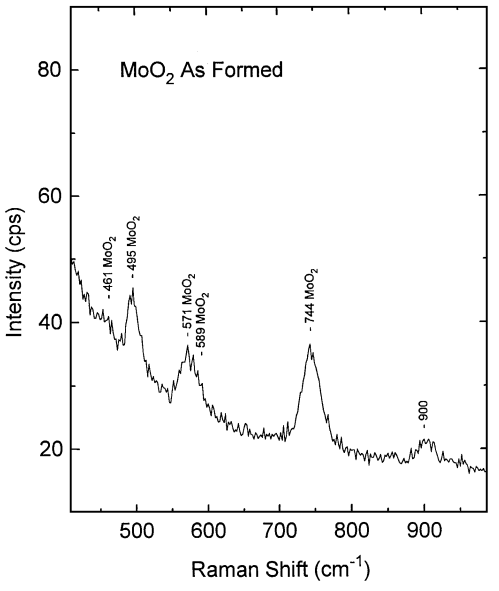

FIG. 3. Raman spectra of the MoO_2 film formed by oxidizing a molybdenum foil in 3×10^{-5} Torr of oxygen at 1130 K for 185 s.

the molybdenum detected in XPS is metallic after heating to this temperature, both Auger and ultraviolet photoelectron spectroscopy reveal the presence of oxygen on the surface which is, in this case, present as an atomic, chemisorbed overlayer which is not completely thermally removed until the sample is heated to ~2000 K. Also shown in Fig. 3 is a Raman spectrum of a film formed by similarly oxidizing a metallic molybdenum foil in the ultrahigh vacuum portion of the apparatus. The spectra were obtained *ex situ* by removing the sample from the manipulator and transporting it in an evacuated desiccator to the Raman spectrometer and collecting the spectrum. This spectrum exhibits features at 461, 495, 571, 589, ad 744 cm^{-1} which have previously been shown to be characteristic of MoO_2 (42, 43, 46–48). Figure 4

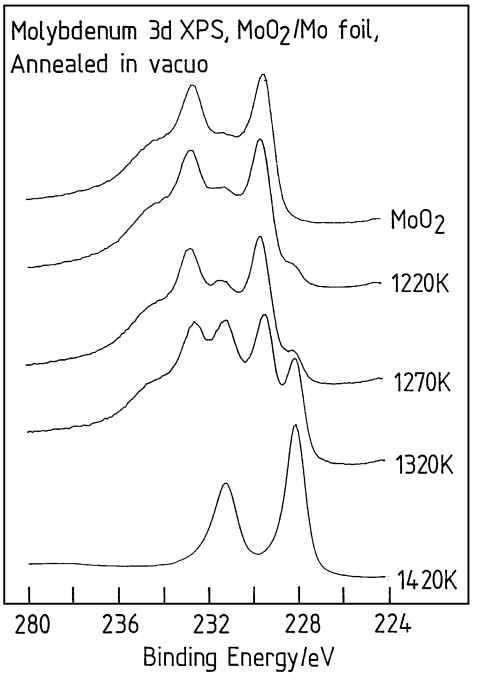

FIG. 2. X-ray photoelectron spectra of a molybdenum foil oxidized in 3×10^{-5} Torr of oxygen at 1130 K for 185 s (top spectrum) and then annealed to various temperatures. The annealing temperature is marked adjacent to each of the spectra.

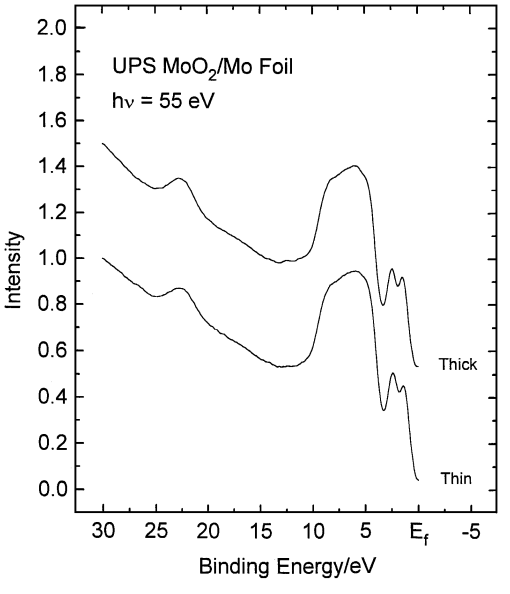

FIG. 4. Ultraviolet photoelectron spectrum of a "thick" MoO_2 film obtained by oxidizing a molybdenum foil in 3×10^{-5} Torr of oxygen at 1130 K for 185 s and a "thin" MoO_2 film obtained by heating a molybdenum foil in 3×10^{-5} Torr of oxygen at 1130 K for 70 s obtained using 55-eV photons.

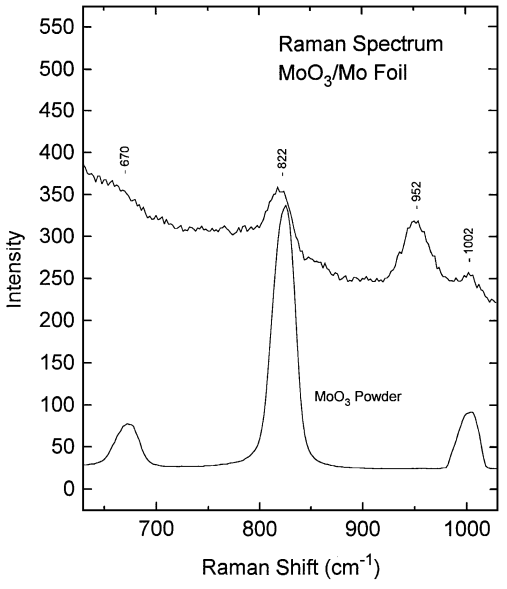

FIG. 5. Raman spectra of the MoO_3 film formed by oxidizing a molybdenum foil in 200 Torr of oxygen in the high-pressure reactor at 550 K for 4 h. Shown for comparison is a Raman spectrum of MoO_3 powder.

displays the ultraviolet photoelectron spectrum of both a "thin" and a "thick" film of MoO_2 obtained by oxidation of a molybdenum sample in ultrahigh vacuum using 3×10^{-5} Torr of oxygen with the sample heated to 1130 K. The thin sample was made by heating for 70 s (where the XPS data of Fig. 1 show metallic molybdenum), and the thick sample was made by oxidation for 185 s (where the data of Fig. 1 reveals only MoO_2). Both of these spectra are essentially identical, showing peaks at 22.7-eV BE due to emission from the O 2*s* orbital and a broad feature centered at ~6.3-eV BE due to emission from the O 2*p* levels. The features within ~4 eV of the Fermi level (E_f) are due to emission from molybdenum *d* bands of the oxide. The sampling depth of photoelectron spectroscopy depends primarily on the kinetic energy of the photoemitted electron (49). In the case of XPS (Fig. 1), this is ~1000 eV, and for UPS (Fig. 4) this is ~30 eV. The mean free path for ~1-kV electrons (~20 Å) is substantially larger than that for ~30-eV electrons (~3 Å). The similarity between the UPS spectra for the thick and thin films in Fig. 4 indicate that a uniform MoO_2 film grows over the metallic molybdenum and the metallic peaks evident in the data in Fig. 1 are just due to the underlying metal detected because of the larger electron mean-free path in this case.

MoO_3 is synthesized at higher pressures using 200 Torr of oxygen with a sample temperature of 550 K (42, 43). This procedure has been demonstrated to be sufficiently vigorous to lead to the complete oxidation of molybdenum metal to MoO_3. This is also illustrated by the Raman spectrum displayed in Fig. 5 which exhibits features at 670, 822, and 1002 cm^{-1}. Shown for comparison is a Raman spectrum of powdered MoO_3 (Mallinckrodt, 99.9% purity) obtained using the same spectrometer. Both of these spectra are in good agreement with each other as well as with previously published spectra of MoO_3 (42, 43), confirming that the *in situ* treatment of metallic molybdenum leads to the formation of molybdenum trioxide. The origin of the feature at 952 cm^{-1} has been assigned to the Mo=O mode of an amorphous phase of MoO_3 (50). The corresponding Mo_2O and Mo_3O modes should be at 868 and 700 cm^{-1}, respectively. The shoulder seen on the 822 cm^{-1} peak in Fig. 5 between 850 and 880 cm^{-1} may be the 868 cm^{-1} mode. The 700 cm^{-1} mode is too weak to see. The structure of this MoO_3 phase is not entirely clear, but is thought to be an octahedrally coordinated hydrated molybdate species. The three modes for this species are analogous to the 1002, 822, and 670 cm^{-1} modes of crystalline MoO_3 (50, 80–82). A peak near 940 cm^{-1} has also been observed for an octahedrally coordinated polymolybdate species supported on AlO_3 under dehydrated conditions; however, the associated peak at 590 cm^{-1} for this phase cannot be resolved (83). As a final check, comparison of the O/Mo Auger ratios of both samples corresponds very well to their relative stoichiometries, which also served as a convenient method for periodically checking the nature of the model catalysts.

Catalytic Activity of Model Catalysts

The rate of propylene metathesis was measured from the slope of the product accumulation curve for the various model oxides. Note that an induction period was found in the rate of olefin metathesis, as illustrated in Fig. 6, which displays the concentration of metathesis products as a function of time for reaction of 450 Torr of propylene at a

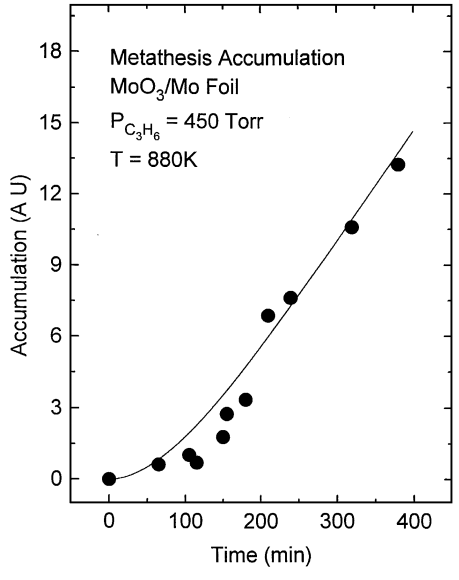

FIG. 6. Typical product accumulation curve for the formation of metathesis products using a model MoO_3 catalyst for reaction at 880 K using a propylene pressure of 450 Torr.

catalyst temperature of 880 K using a model MoO_3 catalyst. The reaction rate (measured from the slope of the curve) is initially rather low and increases as a function of time on stream. Reaction rates presented below are those after the completion of any induction period. Possible origins for this induction period will be discussed below. Note that induction periods in the metathesis of olefins have been noted previously (51, 52).

The reaction temperatures used in these experiments are substantially higher than those conventionally used for olefin metathesis catalyzed by supported oxides, which are usually <650 K. Reactions were carried out, in this case, above this temperature for comparison with the data for metallic molybdenum, which is rather inactive for olefin metathesis until heated to such high temperatures. In addition to the formation of metathesis products, hydrogenolysis products (CH_4 and C_2H_4) were also detected in the reaction products. Similar hydrogenolysis products have been noted for the reaction of metallic molybdenum (23).

The relative activities of each of the model catalysts are displayed in Fig. 7 in histogram form for propylene metathesis on each of the model samples for reaction at 870 K using 450 Torr of propylene. Rates are given in reactions/site/s, where a site is taken to be an exposed molybdenum atom on the (100) face of molybdenum for metallic molybdenum. Since the catalyst was, in this case, a foil, this yields only an approximate value of the number of exposed molybdenum atoms. In the case of MoO_2 and MoO_3, the molybdenum surface concentration was measured from the molybdenum Auger signals relative to that for the metal for each of the model oxide catalysts. These results show that metallic molybdenum is relatively inactive for olefin metathesis, even at such elevated temperatures. MoO_2 is the most active catalyst and MoO_3 shows some intermediate activity (53, 54). Note, however, that it is shown below that MoO_3 is partially reduced to MoO_2 under the reaction conditions, so that the activity data for an initially formed molybdenum trioxide are in fact, for some lower oxidation state oxide. Molybdenum dioxide is stable under these conditions (see Refs. 42, 43, and below).

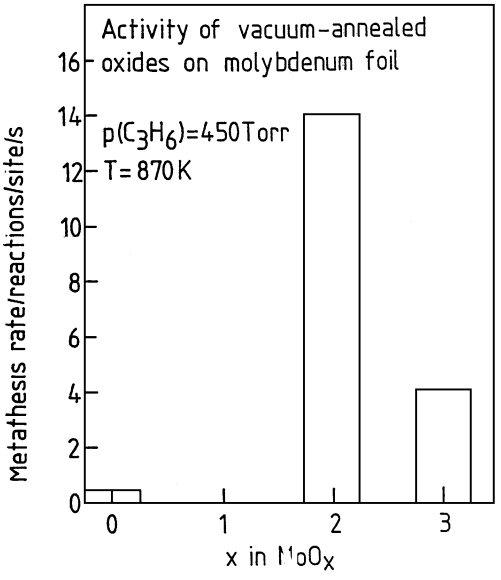

FIG. 7. Histogram displaying the relative catalytic activity for olefin metathesis for model molybdenum metal, MoO_2, and MoO_3 catalysts for the reaction of 450 Torr of propylene at 870 K.

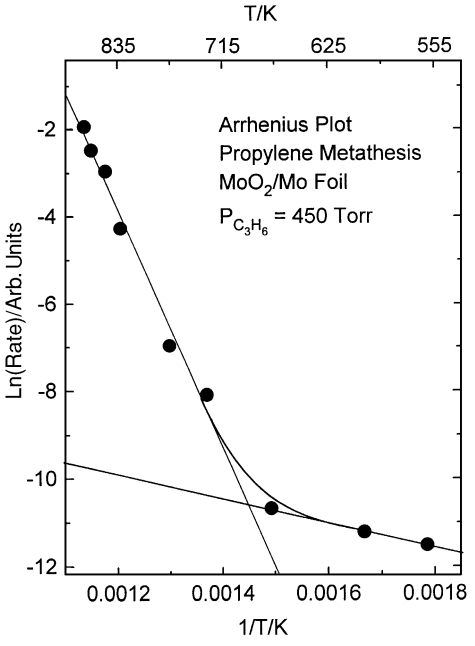

FIG. 8. Temperature dependence of the rate of olefin metathesis using 450 Torr of propylene catalyzed by a model MoO_2 catalyst plotted in Arrhenius form (ln(rate) versus $1/T$).

The temperature dependence of the most active MoO_2 catalyst was measured and the resulting data are displayed in Arrhenius form in Fig. 8 and yield two distinct activation energies. At higher temperatures (>650 K), the activation energy for the reaction is $\sim 63 \pm 5$ kcal/mol, a value very similar to that measured on metallic molybdenum (23). At lower temperatures (<650 K), the activation energy is considerably lower (6 ± 2 kcal/mol). This value is typical for olefin metathesis catalyzed by supported molybdenum oxides (57, 58). It is important to keep in mind that all of these experiments were performed on the same molybdenum foil sample. After each reaction the sample is cleaned and a fresh layer of MoO_2 is deposited on the Mo substrate according to the protocol outlined above.

Displayed in Fig. 9 is the selectivity for olefin metathesis as a function of temperature, where the selectivity S is defined as

$$S = \frac{R_M}{R_M + R_H},$$

where R_M is the rate of metathesis and R_H the rate of

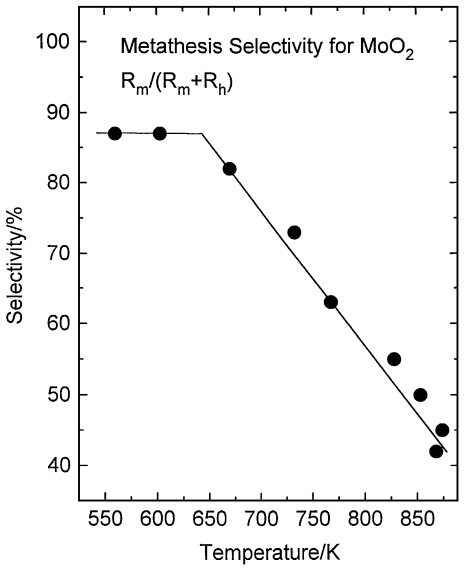

FIG. 9. Temperature dependence of the selectivity to propylene metathesis using 450 Torr of propylene catalyzed by a model MoO_2 catalyst.

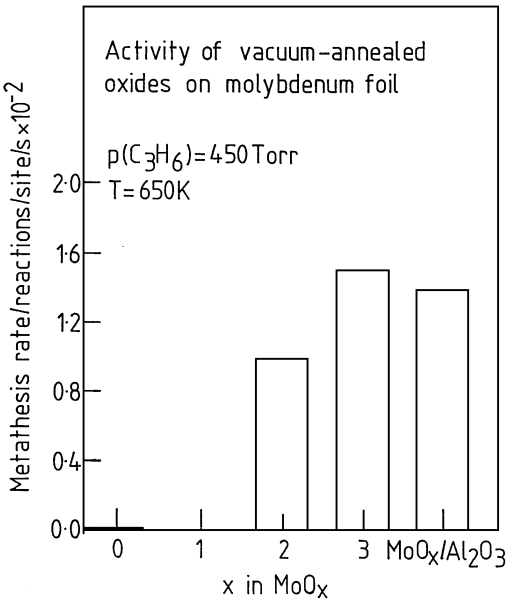

FIG. 10. Histogram displaying the relative catalytic activity for olefin metathesis for model molybdenum metal, MoO_2, and MoO_3 catalysts for the reaction of 450 Torr of propylene at 650 K. Shown for comparison is the corresponding activity for high loadings on molybdenum oxide supported on alumina (see text).

hydrogenolysis (ethylene plus methane formation rate). The metathesis selectivity is constant and relatively high (~87%) for reaction below ~650 K and decreases linearly for reaction above this temperature. This provides additional evidence for different reaction pathways that predominate below and above 650 K.

These results indicate that there are two different reaction pathways leading to the formation of metathesis products. One is a high-activation-energy pathway which predominates at high temperatures, and the other is a significantly lower activation energy route which therefore becomes the most important as the temperature is lowered. Note that olefin metathesis using supported catalysts is usually carried out at temperatures less than 650 K. The correspondence between activation energies measured for supported catalysts and for MoO_2 in this case suggests that similar reactions are being probed in both cases. Further confirmation of this notion comes from Fig. 10, which displays the relative activities of the model catalysts using 450 Torr of propylene at a reaction temperature of 650 K. In this case, metallic molybdenum is essentially completely inactive, while both MoO_2 and MoO_3 show significant activity, with MoO_3 apparently being slightly more active than MoO_2. This calculation of absolute rate assumes that an active site is formed for each available molybdenum atom, and therefore represents a lower bound for the true turnover frequency. The actual identity of the active site for catalysis is not certain. Also shown for comparison is the reaction rate extrapolated to similar conditions for high loadings (18.6%) of molybdenum oxide supported on alumina (2). Not only is the activation energy of the model MoO_2 catalyst similar to that of supported catalysts, but the absolute rates agree very well. This suggests that MoO_2 (and perhaps MoO_3) are the most active forms of the model catalyst and that a thin film of the oxide grown on a metallic substrate provides a good model system for this catalyst. Figure 11 displays a typical product accumulation curve for olefin metathesis at 600 K using 450 Torr of propylene which is, in this case, linear and exhibits no induction period as was noted for reaction at higher temperatures.

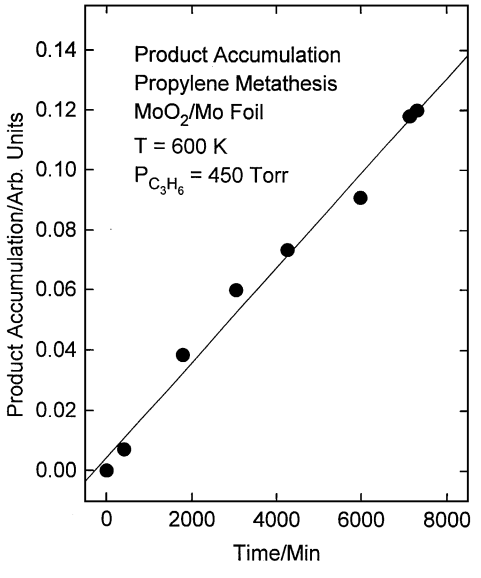

FIG. 11. Product accumulation curve for olefin metathesis catalyzed by MoO_2 for reaction at 600 K using 450 Torr of propylene.

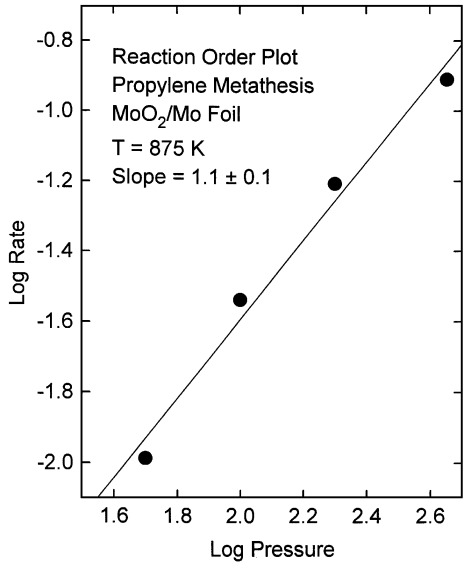

FIG. 12. Pressure dependence of olefin metathesis catalyzed by MoO_2 at 875 K plotted as log(rate) versus log(pressure) where this refers to the propylene pressure.

The pressure dependence of the olefin metathesis rate for reaction at ~880 K is displayed in Fig. 12 in logarithmic form. Measurement of the slope of this curve yields an order for the reaction of 1.1 ± 0.1, so that the reaction is first order in propylene pressure. These kinetic parameters are very similar to those measured for metallic molybdenum (23), implying that similar reaction pathways operate in both regimes.

Nature of the Catalysis Surface during Reaction

It is possible that the surface of the catalysts may become modified during reaction. These effects can be probed using a high-pressure reactor/ultrahigh vacuum system by removing the sample from the reactor to the vacuum portion of the apparatus without any intervening exposure to air. It has been noted previously that molybdenum-catalyzed hydrocarbon conversion reactions proceed in the presence of a carbonaceous deposit (23, 59). This has been found at relatively high temperatures during olefin metathesis (23) but also at considerably lower temperatures for ethylene hydrogenation (59). Similar thick layers of carbonaceous deposit are found on the surfaces on the catalyst after reaction in this case. Plotted in histogram form in Fig. 13 is the amount of carbon found on metallic molybdenum, MoO_2, and MoO_3 model catalysts after reaction in 200 Torr of propylene at 880 K. In all of these cases, the amount of carbon on the surface was measured from the C/Mo Auger ratio which was converted into approximate carbon film thickness using a method that has been described previously (23). Clearly there is a large amount of carbon present on the surface during reaction, although the amount of carbon on the surface decreases substantially as the oxidation state increases, so that clearly one effect of changing the oxidation state is to diminish the amount of carbon on the surface during reaction. It has also been demonstrated using restart reactions that, in the case of metallic molybdenum, at least, the catalytic reaction proceeds in the presence of such a layer (23, 59). In this case, the reaction rate was measured for an initially clean sample. The sample was then removed from the high-pressure reactor into the ultrahigh vacuum portion of the apparatus and the amount of carbon on the surface measured using Auger spectroscopy. The sample was then reinserted into the high-pressure reactor, without any intervening treatment, and the reaction restarted using fresh propylene. Identical reaction rates were measure in both cases, suggesting that the reaction was able to proceed in the presence of such a thick carbonaceous layer. The results of a similar experiment are shown in Fig. 14 where product accumulation curves for the freshly prepared MoO_2 catalyst (Fig. 14, ■) also display an induction period. The corresponding curve after the sample had been removed to ultrahigh vacuum and reinserted into the high-pressure reactor (Fig. 14, ●) displays no induction period and the reaction rate is essentially identical to that in the initial experiment on clean MoO_2 after completion of the induction period. this similarly indicates that the olefin metathesis reaction again proceeds in the presence of a thick carbonaceous layer on the oxide catalyst, although the layer appears to be somewhat thinner in this case. These results also indicate that whatever changes that are associated with the catalytic induction period remain when the sample is removed from the high-pressure reactor into ultrahigh vacuum and after reinsertion into the cell. This effect could be either the formation of some surface species on the catalyst or some change (activation) of the

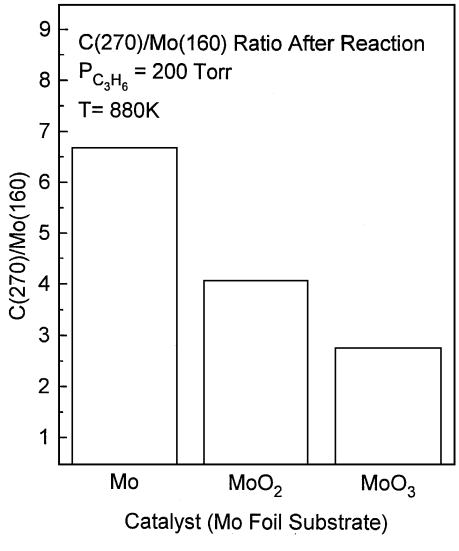

FIG. 13. Histogram comparing the relative amounts of carbonaceous deposit on model Mo, MoO_2, and MoO_3 catalysts following reaction in 200 Torr of propylene at 880 K.

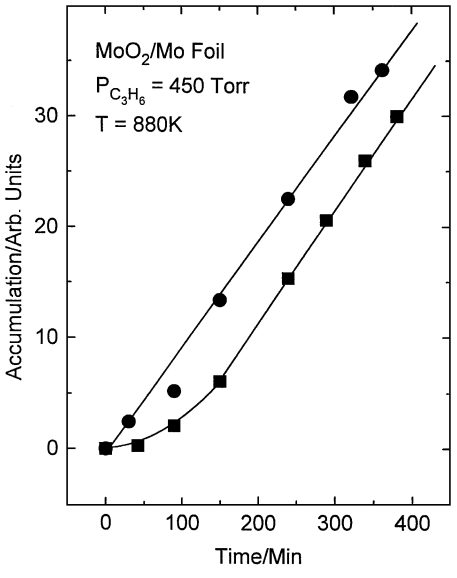

FIG. 14. Product accumulation curve for the metathesis of 450 Torr of propylene at 880 K using a model MoO_2 catalyst: (■) freshly prepared catalyst, (●) after removal into ultrahigh vacuum and reinsertion into the vacuum system.

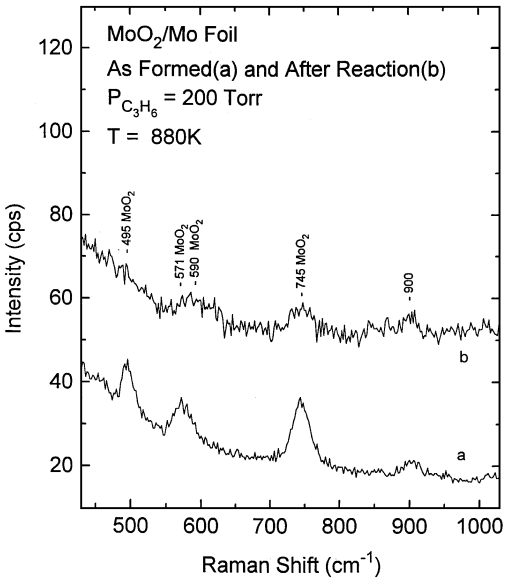

FIG. 16. Raman spectrum of a model MoO_2 catalyst (a) before reaction and (b) after reaction in 200 Torr of propylene at 880 K for 30 min.

catalyst itself. Raman spectroscopy was used to probe the nature of the oxide since the presence of such a thick carbonaceous layer on the catalyst sample following reaction means that the substrate oxide is rather difficult to follow using other, more surface-sensitive methods such as X-ray photoelectron spectroscopy, whereas Raman spectroscopy probes the whole of the film. The resulting Raman spectra of the model MoO_3 catalyst prior to reaction is displayed in Fig. 15a showing the characteristic Raman peaks of the trioxide (42, 43). Figure 15b displays the corresponding region of the spectrum after reaction in 200 Torr of propylene at 880 K. The peaks due to MoO_3 are essentially absent following reaction with propylene and additional features are present due to the formation of MoO_2 (42, 43, 46–48). That is, the initially formed model molybdenum trioxide catalyst had been reduced during reaction to form molybdenum dioxide. These results are in good agreement with the work of others to examine the reducibility of oxidized molybdenum catalysts which have similarly shown the reduction of MoO_3 to MoO_2 under comparable conditions in hydrogen (42, 43, 55, 56).

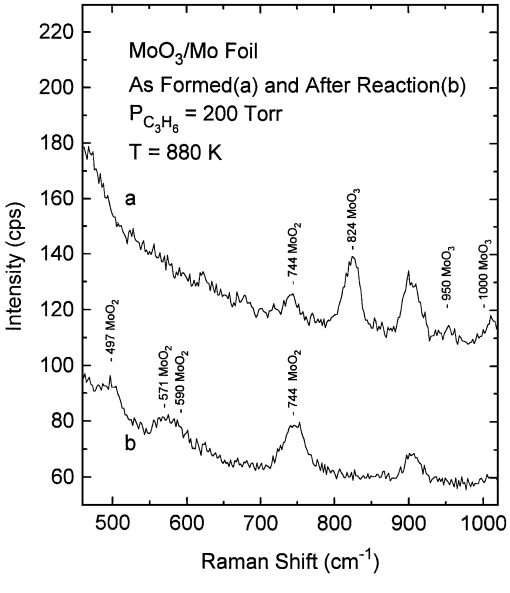

FIG. 15. Raman spectrum of a model MoO_3 catalyst (a) before reaction and (b) after reaction in 200 Torr of propylene at 880 K for 30 min.

The results of a similar set of experiments for metathesis catalyzed by MoO_2 are displayed in Fig. 16; the Raman spectrum of MoO_2 is shown in Fig. 16a (42, 43, 46–48), confirming that MoO_2 had indeed been formed, and Fig. 16b shows the corresponding spectrum after reaction. No further reduction in the sample is apparent, although the spectrum is attenuated in intensity, probably due to the presence of the carbonaceous layer present on the sample. This result is again in accord with those of previous experiments which have shown that, under similar conditions, MoO_3 reduces primarily to MoO_2 (42, 43, 55, 56).

The origin of the feature at ~900 cm^{-1} in Figs. 15 and 16 is unclear. There is evidence in the literature for both tetrahedrally and octahedrally coordinated molybdate species having peaks near this region (80–82). It is possible that this mode and the other surface molybdate mode observed (950 cm^{-1}) may have formed from water contamination during *ex situ* Raman analysis. It seems unlikely that hydrated molybdate species would form during preparation in ultrahigh vacuum, and formation during reaction may be

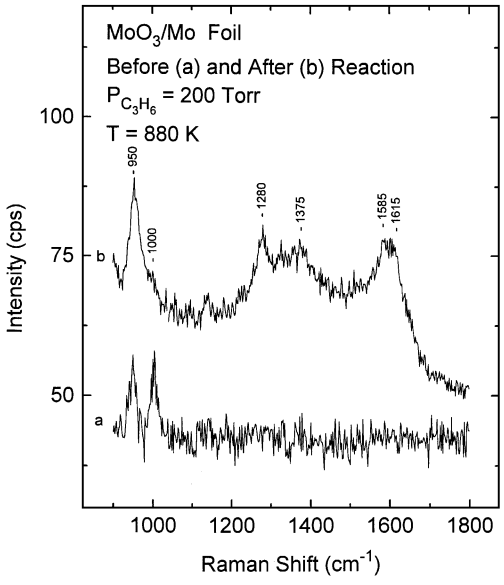

FIG. 17. Raman spectrum of a model MoO_3 catalyst displaying the region of the spectrum between 900 and 1800 cm^{-1} before (a) and after (b) reaction in 200 Torr of propylene at 880 K for 30 min.

ruled out since these features appear on catalysts not used for reaction.

Finally, additional features were found in the Raman spectrum of the MoO_2 sample after reaction (which were not present prior to catalysis). These are displayed in Fig. 17 for the region between 900 and 1800 cm^{-1} and in Fig. 18 for the region between 2700 and 3300 cm^{-1} and show features around 3000 cm^{-1} and around 1600 cm^{-1}. These are assigned to vibrational modes of absorbed hydrocarbons (60). In view of the relatively large amount of carbon detected on the surface following reaction using Auger spectroscopy, it is suggested that these features are due to these carbonaceous species and indicate that they consist substantially of adsorbed hydrocarbons. Note that the restart reactions described above on MoO_2 and other such experiments on metallic molybdenum indicate that catalysis proceeds in the presence of such a carbonaceous layer. This phenomenon has been seen previously where, for example, ethylene hydrogenation catalyzed by metallic platinum was found to proceed in the presence of an overlayer of ethylidyne (61). In addition, a similar hydrocarbon layer was also found for the same reaction catalyzed by metallic molybdenum, except in this case the carbonaceous layer thickness was much greater for the metallic molybdenum catalyst than for platinum (23, 59).

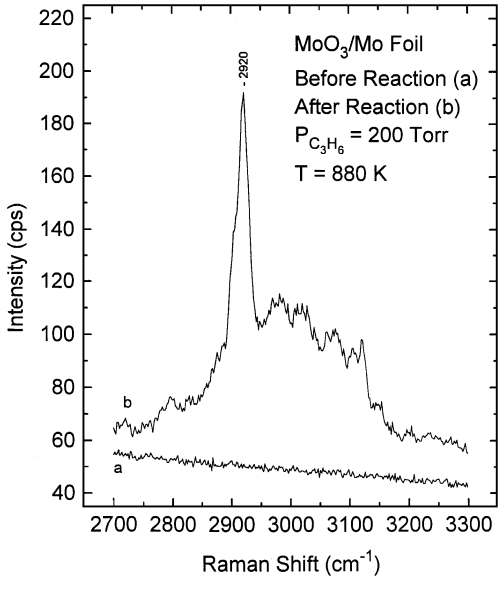

FIG. 18. Raman spectrum of a model MoO_3 catalyst displaying the region of the spectrum between 2700 and 3300 cm^{-1} before (a) and after (b) reaction 200 Torr of propylene at 880 K for 30 min.

DISCUSSION

X-ray photoelectron (Figs. 1 and 2), Raman (Figs. 3 and 5), and ultraviolet photoelectron (Fig. 4) spectroscopies demonstrate that films of MoO_2 and MoO_3 can be grown by the oxidation of metallic molybdenum. MoO_2 is grown by controlled oxidation in ultrahigh vacuum and MoO_3 is synthesized by oxidation at higher pressures using the isolatable reactor. Metallic molybdenum can be formed rather easily by cleaning metallic molybdenum in ultrahigh vacuum using well-established techniques. The MoO_2 layer is thermally rather stable is ultrahigh vacuum (Fig. 2) and can be heated to ~1200 K without thermally decomposing. This thermal stability is maintained even in a reducing atmosphere at 880 K since the Raman spectrum after reaction under these conditions is essentially identical to that found prior to reaction (Fig. 6). The same is not true for MoO_3 which is reduced to MoO_2 by reaction in propylene at 880 K (Fig. 15). These results are in accord with those found in other studies of the reducibility of molybdenum oxides (42, 43, 55, 56).

The relative activities of the model catalysts at high reaction temperatures (~880 K) show strong variation with oxidation state (Fig. 7) as has been found previously for supported molybdenum oxide catalysts (53, 54). Note, however, that the reactivity for a catalyst initially comprising MoO_3 is reduced under reaction conditions. In addition, an induction period is found for the reaction on both MoO_3 (Fig. 3) and MoO_2 (Fig. 14); it is tempting to associate with the reduction of the MoO_3 sample, and clearly this may contribute to this effect. However, a similar induction period is also evident for the metathesis catalyzed by MoO_2 which is not reduced similarly, which suggests that there is another origin for the induction period. This will be discussed in greater detail below. The activation energy of the reaction at these high temperatures is considerably larger

than conventionally encountered for olefin metathesis using supported molybdenum oxide catalysts and is close to that found for metallic molybdenum (23). In contrast, reaction at lower temperatures (<650 K) proceeds with an activation energy more closely akin to that found for supported catalysts (Fig. 8) (57, 58) and, moreover, the absolute reaction rates for both MoO_2 ad MoO_3 are in good agreement with high loadings (18.6%) of molybdenum oxide on alumina (2) (Fig. 10). In addition, the reaction selectivity is high (∼90%) and rather constant for reaction below ∼650 K but decreases linearly with increasing temperature above this value (Fig. 9). These results suggest that films of molybdenum oxide provide a good model for the supported metathesis catalysts at high loadings for reaction below ∼650 K where the surface of the alumina support is likely completely covered by the oxide. Under these conditions, it is clear that metallic molybdenum is completely inactive for the metathesis of olefins while both MoO_3 and MoO_2 show similar activities. This result agrees with what has been observed previously for supported Mo catalysts, where Mo(0) is found to be essentially inactive for metathesis and oxidized molybdenum at high loading exhibits some metathesis activity (83). Note also that no induction period is found for reaction at these lower temperatures. These results suggest that there are two distinct metathesis pathways which proceed simultaneously: a high-activation-energy (∼65 kcal/mol) route that predominates above ∼650 K and a lower-activation-energy route (∼6 kcal/mol) that operates below this temperature. As mentioned above, the activation energy, absolute rate, and selectivity for metathesis in the low-temperature regime are akin to those measured for supported oxides. In addition no induction period is found for the low-temperature reaction (Fig. 11). It has been suggested that the reaction pathway at these lower temperatures proceeds via the initial formation of a carbene "active site." This has been proposed to react further with an alkene forming a metallacycle which can then decompose via the reverse of this reaction pathway to yield metathesis products via a two-step reaction (6–22). It is likely that this reaction pathway operates at lower reaction temperatures (<650 K) but that another, much higher-activation-energy route, predominates as the temperature increases. It should be emphasized that both reactions proceed simultaneously and that it is the vast differences in activation energies for the two pathways which cause one or the other to predominate in different temperature regimes.

The reaction kinetics (both pressure dependence (Fig. 12) and activation energy (Fig. 8)) are similar for the oxides and metal for reaction at high temperatures (>650 K) (23). This suggests that the reaction pathway may be identical for these catalysts at high temperatures. It should also be noted that metallic molybdenum model catalysts are active for hydrocarbon formation from CO and hydrogen (Fisher–Tropsch synthesis) (62) and in this case, the reaction proceeds via polymerization of adsorbed CH_x species (63–70). In this context, we have recently examined the reaction of ethylene catalyzed by metallic molybdenum at temperatures above 650 K (71, 72). In this case, the metathesis of ethylene is degenerate since it should yield only ethylene. However, higher hydrocarbons up to C_6 are also detected in the reaction products for reaction above ∼650 K, suggesting that carbenes can recombine, forming higher-molecular-weight products in this temperature region. It is thus proposed that metathesis takes place at higher temperatures via recombination of the carbene fragments on the surface and that this reaction proceeds in parallel with the lower activation energy route but with an activation energy of ∼65 kcal/mol. Such a reaction route has been proposed previously as one of the removal pathways for carbene species from the surface during olefin metathesis (73).

A common feature of catalysis, in the case of both metals and oxides, is the presence of a carbonaceous deposit on the surface following reaction. Restart reactions (Fig. 4) indicate that reaction takes place in the presence of these carbonaceous deposits. They are sufficiently thick that they can be detected using Raman spectroscopy (Figs. 17 and 18) and exhibit C-H stretching modes in the region 2800 to 3100 cm^{-1} (60) at 2797, 2923, 2983, 3019, 3076, and 3116 cm^{-1}, indicating that they indeed consist of hydrocarbon fragments on the surface rather than carbonaceous deposits. The most prominent feature in this region is at 2923 cm^{-1} which can be assigned to the asymmetric stretching mode of a $-CH_2-$ species, suggesting that the adsorbed hydrocarbon is predominantly saturated. The corresponding symmetric stretching mode should be at ∼2850 cm^{-1} and, although there is some intensity in this region, it is rather weak. The corresponding bending modes for methylene species are at ∼1300 cm^{-1} and a feature is evident at ∼1280 cm^{-1} (Fig. 17). The peak at ∼2980 cm^{-1} may be due to the asymmetric stretching mode of a methyl group which is much weaker than the corresponding methylene mode consistent with a relatively long hydrocarbon chain. The corresponding symmetric stretch should appear at ∼2870 cm^{-1} and the shoulder on the lower frequency side of the main 2923 cm^{-1} feature may be due to this mode. The corresponding bending modes should appear at ∼1380 and 1460 cm^{-1} and may form part of the broad feature between 1250 and 1650 cm^{-1} in Fig. 17. The possible origin of these features will be discussed in greater detail below. The higher frequency features in the C–H stretching region (evident at 3019, 3076, and 3116 cm^{-1}) may be indicative of some olefinic bonds in the adsorbed hydrocarbon (74–77).

The Raman spectrum of small graphitic particles exhibits broad features at ∼1600 and 1350 cm^{-1} (78, 79). The broad feature at ∼1600 cm^{-1} (Fig. 17) may be due to the presence of some graphitic species on the surface. The corresponding

feature at ~1350 cm^{-1} has narrower peaks superimposed on it which have been discussed above.

In view of the fact that reaction products are found due to polymerization of carbonaceous fragments on the surface, these surface hydrocarbons may also be formed by a similar route. Note that they are present at some equilibrium thickness since restart reactions were carried out after many turnovers (in excess of 20,000 in the case of the data shown in Fig. 14) had been completed and the reaction proceeded at a constant rate when the carbon-covered surface was reinserted into the reaction cell (Fig. 14). If the amount of carbon on the surface was continually increasing, this would likely result in a continuous decrease in the rate of the catalytic reaction with time on stream. Such a carbonaceous layer has also been detected during ethylene hydrogenation catalyzed by Mo(100) and appears to be a common feature of transition-metal and also transition-metal-oxide-catalyzed hydrocarbon reactions. Note that the films found on molybdenum and molybdenum oxides are considerably thicker than those found on Group VIII metals, so that, for example, ethylene hydrogenation proceeds on platinum in the presence of a monolayer of adsorbed ethylidyne. It is probable that the presence of such a layer has the effect of inhibiting catalysis both by blocking sites and by impeding access to the surface. It is likely that the thicker layer found for molybdenum catalysts also contributes to their relatively low activity, for example, for ethylene hydrogenation compared to platinum. It is difficult, however, to extrapolate these conclusions regarding the presence of a carbonaceous layer to the performance of supported molybdenum catalysts due to the significant difference between the reaction conditions investigated here and the actual conditions under which supported catalysts are used.

Finally, we turn our attention now to the nature of the induction period observed at high temperatures (>650 K) for olefin metathesis (51, 52). Note that no such induction period is found for reaction at lower temperatures on any of the oxides, or on the metal surface when used as a metathesis catalyst. This suggests then that the accumulation of carbonaceous deposits is not responsible for the induction period since such deposits are found on catalysts that do not exhibit the effect, for example, metallic molybdenum. It would also be expected that accumulation of carbonaceous deposits would, in contrast to experimental observations, lead to a decrease rather than an increase in activity with time on stream. The other change that has been noted during the reaction is a reduction in oxidation state from +6 to +4 for the MoO_3 catalyst, and the induction period may reflect the transformation from an inactive MoO_3 to a more active MoO_2 catalyst. This would explain the absence of an induction period on metallic molybdenum (since this is not reducible) and at lower reaction temperatures (since the catalyst is not reduced). However, an induction period was also found for metathesis catalyzed by MoO_2 above 650 K, whereas Raman data and previous work indicate that the bulk of the catalyst is not reduced under these conditions. A possible explanation may be that the outer portion of the MoO_2 catalyst is reduced during reaction and that the induction period reflects this reduction of the surface atoms, whereas the bulk of the sample remains as an oxide.

CONCLUSIONS

Model catalysts can be synthesized that consist of metallic molybdenum, MoO_2, and MoO_3. Variations in activity for olefin metathesis are found as a function of sample oxidation state where MoO_2 is found to be the most active above ~650 K and both MoO_2 and MoO_3 are active for reaction below ~650 K and where the kinetics resemble those of high loadings (18.6%) of an oxide on an alumina support. Catalysts are characterized using ultraviolet and X-ray photoelectron and Raman spectroscopies which confirm the formation of the model oxides, and Raman spectroscopy demonstrates that MoO_3 is reduced during reaction at high temperatures.

A thick carbonaceous layer is found on the surface of the catalysts during reaction at high temperature, and restart reactions confirm that catalysis proceeds in the presence of this film. Raman spectra of the film indicate that it consists of a hydrocarbon anchored to the surface of the catalysts. An induction period is found in the rate of metathesis at high temperatures and this is tentatively assigned to a reduction of the outermost layer of the catalyst during reaction.

ACKNOWLEDGMENTS

We gratefully acknowledge support of this work by the U.S. Department of Energy, Division of Chemical Sciences, Office of Basic Energy Sciences, under Grant DE-FG02-92ER14289. This work is based upon research conducted at the Synchrotron Radiation Center, University of Wisconsin–Madison, which is supported by the NSF under Award DMR-95-31009.

REFERENCES

1. Banks, R. L., and Bailey, G. C., *Ind. Eng. Chem., Prod. Res. Dev.* **3**, 170 (1964).
2. Calderon, N., Chen, H. Y., and Scott, K. W., *Tetrahedron Lett.* **8**, 3327 (1967).
3. Brenner, A., and Burwell, R. L., Jr., *J. Catal.* **52**, 364 (1978).
4. Millman, W. S., Crespin, M., Cirrillo, A. L., Abdo, S., and Hall, W. K., *J. Catal.* **60**, 404 (1979).
5. Thomas, R., and Moulijn, J. A., *J. Mol. Catal.* **15**, 157 (1982).
6. Hérisson, J. L., and Chauvin, Y., *Makromol. Chem.* **141**, 161 (1970).
7. Soufflet, J. P., Commercue, D., and Chauvin, Y., *C. R. Hebd. Séances Acad. Sci. Ser. C.* **276**, 169 (1973).
8. Haines, R. J., and Leigh, G. J., *Chem Soc. Rev.* **4**, 155 (1975).
9. Casey, C. P., and Burkhardt, J., *J. Am. Chem. Soc.* **96**, 7808 (1974).
10. Fischer, E. O., and Dotz, K. H., *Chem. Ber.* **105**, 3966 (1972).
11. Schrock, R. R., *J. Am. Chem. Soc.* **96**, 6976 (1974).
12. Schrock, R. R., *J. Am. Chem. Soc.* **98**, 5399 (1976).
13. Dolgoplosk, B. A., *Dokl. Chem.* **216**, 380 (1974).

14. Grubbs, R. H., Burk, P. C., and Carr, D. D., *J. Am. Chem. Soc.* **97**, 3265 (1975).
15. Grubbs, R. H., Carr, D. D., Hoppin, C., and Burk, P. C., *J. Am. Chem. Soc.* **98**, 3478 (1976).
16. Katz, T. J., and Rothschild, J., *J. Am. Chem. Soc.* **98**, 2519 (1976).
17. Katz, T. J., and Hersch, W. H., *Tetrahedron Lett.* 585 (1977).
18. Casey, C. P., Hunstra, H. E., and Searnan, M. C., *J. Am. Chem. Soc.* **98**, 608 (1976).
19. Tebbe, F. N., Parshall, G. W., and Overnall, D. W., *J. Am. Chem. Soc.* **98**, 608 (1976).
20. Wengorius, J., Schrock, R. R., Churchill, M. R., Mussert, J. R., and Young, W. J., *J. Am. Chem. Soc.* **102**, 4515 (1980).
21. Howard, T. R., Lee, J. B., and Grubbs, R. H., *J. Am. Chem. Soc.* **102**, 6878 (1980).
22. Grubbs, R. H., and Brunck, T. K., *J. Am. Chem. Soc.* **94**, 25 (1972).
23. Wang, L. P., Soto, C., and Tysoe, W. T., *J. Catal.* **143**, 92 (1993).
24. Wang, L. P., and Tysoe, W. T., *J. Catal.* **28**, 320 (1991).
25. Huezo, L. A., Kotvis, P. V., Crumer, C., Soto, C., and Tysoe, W. T., *Appl. Surf. Sci.* **78**, 113 (1994).
26. Wang, L. P., and Tysoe, W. T., *Surf. Sci.* **230**, 74 (1990).
27. Wang, L. P., and Tysoe, W. T., *Surf. Sci.* **236**, 325 (1990).
28. Wang, L. P., and Tysoe, W. T., *Surf. Sci.* **245**, 41 (1991).
29. Lombardo, E. A., Lo Jacono, M., and Hall, W. K., *J. Catal.* **51**, 243 (1978).
30. Chung, J. K., and Burwell, R. L., Jr., *J. Catal.* **116**, 506 (1989).
31. Chung, J. K., and Burwell, R. L., Jr., *J. Catal.* **116**, 519 (1989).
32. Goldwasser, J., Engelhardt, J., and Hall, W. K., *J. Catal.* **71**, 381 (1981).
33. Kennett, H. M., and Lee, A. E., *Surf. Sci.* **48**, 591 (1975).
34. Kennett, H. M., and Lee, A. E., *Surf. Sci.* **48**, 606 (1975).
35. Kennett, H. M., and Lee, A. E., *Surf. Sci.* **48**, 617 (1975).
36. Kennett, H. M., and Lee, A. E., *Surf. Sci.* **48**, 624 (1975).
37. Kennett, H. M., and Lee, A. E., *Surf. Sci.* **48**, 633 (1975).
38. Lee, A. E., *Surf. Sci.* **47**, 191 (1975).
39. Zhang, C., Van Hove, M. A., and Somorjai, G. A., *Surf. Sci.* **149**, 326 (1985).
40. Bauer, E., and Poppa, H., *Surf. Sci.* **88**, 31 (1979).
41. Gotoh, Y., and Yanocura, E., *Surf. Sci.* **287/288**, 979 (1993).
42. Spevack, P. A., and McIntyre, N. S., *J. Phys. Chem.* **96**, 9029 (1992).
43. Spevack, P. A., and McIntyre, N. S., *J. Phys. Chem.* **97**, 11020 (1993).
44. Cimano, A., and Deangelis, B. A., *J. Catal.* **36**, 11 (1975).
45. Haber, J., Marczewski, W., Stoch, J., and Ungier, L., *Ber. Bunsenges. Phys. Chem.* **79**, 970 (1975).
46. Smudde, G. H., and Stair, P. C., *Surf. Sci.* **317**, 65 (1994).
47. Payen, E., Grimblot, J., and Kasztelan, S., *J. Phys. Chem.* **91**, 6642 (1987).
48. Shafer, G. L., and Cheng, C. P., *J. Catal.* **80**, 369 (1983).
49. Ertl, G., and Kuppers, J., "Low Energy Electrons and Surface Chemistry," p. 7. VCH, Weinheim, 1985.
50. Ajito, K., Nagahara, L. A., Tryk, D. A., Hashimoto, K., and Fujiahima, A., *J. Phys. Chem.* **99**, 16385 (1995).
51. Luckner, R. C., and Wills, G. B., *J. Catal.* **28**, 83 (1973).
52. Wills, G. B., Fathikalajahi, J., Gangwal, S. K., and Tang, S., *Rec. Trav. Chim.* **96**, M110 (1977).
53. Burwell, R. L., and Brenner, A. J., *J. Mol. Catal.* **1**, 77 (1975).
54. Thomas, R., and Moulijn, J. A., *J. Mol. Catal.* **15**, 157 (1982).
55. Yamada, M., Yasumaru, J., Houalla, M., and Hercules, D. M., *J. Phys. Chem.* **95**, 7037 (1991).
56. Grünert, W., Stakheev, A. Y., Feldhaus, R., Anders, K., Shapiro, E. S., and Minachev, K. M., *J. Phys. Chem.* **95**, 1323 (1991).
57. Davie, E. S., Whan, D. A., and Kemball, C., *J. Catal.* **24**, 272 (1972).
58. Moffat, A. J., and Clark, A., *J. Catal.* **17**, 264 (1970).
59. Wang, L. P., and Tysoe, W. T., *J. Catal.* **128**, 320 (1991).
60. Bellamy, L. T., "The Infrared Spectra of Complex Molecules," p. 273. Wiley, London, 1960.
61. Zaera, F., and Somorjai, G. A., *J. Am. Chem. Soc.* **106**, 2288 (1984).
62. Logan, M., Gellman, A. J., and Somorjai, G. A., *J. Catal.* **94**, 60 (1985).
63. Goodman, D. W., *J. Vac. Sci. Technol.* **20**, 522 (1982).
64. Goodman, D. W., Kelley, R. D., Madey, T. E., and Yates, J. T., Jr., *J. Catal.* **63**, 226 (1980).
65. Goodman, D. W., Kelley, R. D., Madey, T. E., and White, J. M., *J. Catal.* **64**, 479 (1980).
66. Yamamoto, T., *J. Chem. Soc. Chem. Commun.* 1003 (1978).
67. Young, C. B., and Whiteside, G. N., *J. Am. Chem. Soc.* **100**, 5808 (1978).
68. Ponec, V., and Barneveld, W. A. A., *Ind. Eng. Chem. Prod. Res. Dev.* **18**, 268 (1979).
69. Biloen, P., Helle, J. N., and Sachtler, W. H. M., *J. Catal.* **58**, 95 (1979).
70. Brady, R. C., and Petti, R. J., *J. Am. Chem. Soc.* **102**, 6181 (1981).
71. Bartlett, B., Schneerson, V. L., and Tysoe, W. T., *Catal. Lett.* **32**, 1 (1995).
72. Bartlett, B. F., Soto, C., Molero, H., and Tysoe, W. T., in preparation.
73. Loggenberg, P. M., Carlton, L., Copperthwaite, R. G., and Hutchins, G. J., *J. Chem. Soc. Chem. Commun.* 541 (1987).
74. Colthup, N. B., Daly, L. H., and Wiberly, S. E., "Introduction to Infrared and Raman Spectroscopy." Harper & Row, New York, 1964.
75. Laszlo, P., and Stang, P. J., "Organic Spectroscopy." Harper & Row, New York, 1971.
76. Loader, J., "Basic Laser Raman Spectroscopy." Heyden & Son, London, 1970.
77. Shriner, R. L., Fuson, R. C., and Crutin, D. Y., "The Systematic Identification of Organic Compounds." John Wiley & Sons, New York, 1958.
78. Lespade, P., Al-Jishi, R., and Dresselhaus, M. S., *Carbon* **20**, 427 (1982).
79. Knight, D. S., and White, W. B., *J. Mater. Res.* **4**, 385 (1989).
80. Hu, H., and Wachs, I. E., *J. Phys. Chem.* **99**, 10897 (1995).
81. Payen, E., Kasztelan, S. J., Grimblot, J., and Bonelle, J. P., *J. Raman Spec.* **17**, 233 (1986).
82. Sequin, L., Figlarz, M., Cavagnat, R., and Lasseques, J. C., *Spec. Acta A* **51**, 1323 (1995).
83. Brenner, A., and Burwell, R. B., Jr., *J. Catal.* **63**, 463 (1980).